Published in final edited form as:

J Control Release. 2018 April 10; 275: 85–91. doi:10.1016/j.jconrel.2018.02.008.

Colorectal cancer lung metastasis treatment with polymer–drug nanoparticles

Piotr Rychahou[a,b], **Younsoo Bae**[d], **Derek Reichel**[d], **Yekaterina Y. Zaytseva**[a], **Eun Y. Lee**[a,c], **Dana Napier**[c], **Heidi L. Weiss**[a], **Nick Roller**[a], **Heather Frohman**[a,b], **Anh-Thu Le**[a,b], **B. Mark Evers**[a,b,*]

[a]Markey Cancer Center, The University of Kentucky, Lexington, KY 40536, United States

[b]Department of Surgery, The University of Kentucky, Lexington, KY 40536, United States

[c]Pathology and Laboratory Medicine, The University of Kentucky, Lexington, KY 40536, United States

[d]Department of Pharmaceutical Sciences, The University of Kentucky, Lexington, KY 40536, United States

Abstract

Colorectal cancer (CRC) is the second leading cause of cancer deaths in the United States; the predominant cause for mortality is metastasis to distant organs (e.g., lung). A major problem limiting the success of chemotherapy in metastatic CRC is the inability to target tumor tissues selectively and avoid severe side effects to normal tissues and organs. Here, we demonstrate polymeric nanoparticles (PNPs) entrapping chemotherapeutic agents provide a new therapeutic option for treating CRC that has metastasized to the lung. PNPs assembled from FDA approved biocompatible block copolymer accumulated predominantly in lung tissue. PNPs showed negligible accumulation in liver, spleen and kidneys, which was confirmed by fluorescent nanoparticle imaging and analysis of PI3K inhibition in the organs. PNPs entrapping PI3K inhibitors (i.e., wortmannin and PX866) suppressed CRC lung metastasis growth, and SN-38-loaded PNPs completely eliminated CRC lung metastasis. Our results demonstrate that polymer-drug nanoparticles offer a new approach to reduce toxicity of cancer therapy and has the potential to improve outcomes for patients with lung metastasis.

Keywords

Colorectal cancer; Polymeric nanoparticles; CRC lung metastasis; PI3K inhibitors; Nanoparticle therapeutics

*Corresponding author at: Markey Cancer Center, University of Kentucky; 800 Rose Street, CC140, Lexington, KY 40536, United States. mark.evers@uky.edu (B. Mark Evers).

Supplementary data to this article can be found online at https://doi.org/10.1016/j.jconrel.2018.02.008.

1. Introduction

Colorectal cancer (CRC) is the second leading cause of cancer deaths in the United States and the third most common cancer in men and in women [1]. Approximately 1 in 5 patients with CRC present with distant metastatic disease at diagnosis; relapse after resection will occur in almost 50% of the patients, with a 5-year relapse-free survival rate ranging from 15% to 35% [2,3]. Of the patients with CRC who develop systemic metastasis, 10–15% develop metastases to the lungs [4,5]. In addition to CRC metastasis, the lung is a common site of metastasis for other solid cancers (e.g., bladder, breast, kidney, pancreatic and prostate cancers) [6]. Secondary lung metastasis is a significant problem in the field of cancer. There is a critical need for an affordable and reliable solution to deliver therapeutics to treat lung metastases.

Emerging nanotechnologies promise new treatment approaches for patients with metastatic cancer. The US Food and Drug Administration approved the first such treatment, Doxil, which is the chemotherapy drug doxorubicin packaged in a lipid nanoparticle [7,8]. However, since the approval of Doxil over 20 years ago, the possibility of engineering nanoparticles that selectively detect and destroy cancer cells in the body remains only a concept and the clinical potential of nanotechnology has not been fully realized. Research published over the last decade clearly shows that nanoparticle delivery specifically to cancer cells can increase chemotherapy delivery into tumors while reducing drug accumulation in healthy tissues, but the development of successful nanotechnologies targeting lung metastasis remains an elusive goal [9]. Understanding the limitations of targeting metastatic tumors with nanoparticles and maximizing the existing capabilities of nanoparticle formulations is needed to fill the growing clinical demand for reliable drug delivery strategies [10,11]. Tissue-specific drug delivery *via* PNPs has the potential to provide a clinically relevant tool to address the problems associated with traditional chemotherapy.

Class I phosphoinositide 3-kinase (PI3K) and protein kinase B (Akt) are two major established drivers of oncogenic activity in human malignancy [12–15]. Pharmacologically-active concentrations of drugs in the tumor tissue can only be reached at the expense of PI3K/Akt inhibition in normal tissues unaffected by metastatic disease. This poor specificity creates a serious obstacle to achieve effective antitumor therapy. Another major challenge in advancing novel PI3K/Akt inhibitors into clinical trials is their low solubility in aqueous solutions; intravenous administration of these drugs is challenging and requires a formulation with organic solvents and surfactants. As a result, many promising therapeutics have failed clinical translation and were never considered clinically viable. The development of tissue-selective nanocarriers has the potential to deliver high concentrations of chemotherapeutic agents to target tissues, spare normal organs, and combat multidrug resistance [16,17].

A critical finding of our current study was the ability of PNPs to deliver a high dose of PI3K/Akt inhibitors to lung tissue and lung metastases, and to spare other normal organs (e.g., kidney and liver). The nanoparticles used in this study are composed of PEG-PCL polymer, which is an FDA-approved chemical with well-characterized degradation kinetics

and biocompatibility [18,19]. The development of PNPs has the distinct potential to deliver potent, but highly toxic therapies to treat lung metastases. Our results demonstrate the potential of PNPs for drug delivery and suggest that lung PI3K inhibition is a viable treatment strategy against CRC lung metastasis.

2. Materials and methods

2.1. Cell lines, transfections

HT-29 cells were obtained from American Type Culture Collection (Manassas, VA). Cells were previously authenticated by Genetica DNA Laboratories (Cincinnati, OH) and cultured in McCoy's 5A medium, purchased from Sigma Aldrich (St. Louis, MO) supplemented with 10% FBS and 1% Gibco antibiotic-antimycotic (Thermo Fisher Scientific, Waltham, MA). HT-29 GFP-Luc cell line was established after transfection with EGFP-N1 vector and injection with pGL3 firefly luciferase lentivirus. EGFP-N1 vector was purchased from Clontech (Mountain View, CA). GFP-expressing cells were selected with 500 μg/ml Geneticin (G418), purchased from Life Technologies (Carlsbad, CA) and enriched by three cycles of fluorescence-activated cell sorting (FACS). Pre-made pGL3 firefly luciferase (luc) lentiviral particles were purchased from Lentigen (Gaithersburg, MD). For lentiviral transduction, 5000 cells/well were seeded in 96 well tissue culture plates and infected the following day with luc lentiviral particles at a MOI of 10 in the presence of 10 μg/ml polybrene, purchased from Santa-Cruz Biotechnology (Dallas, TX). Luciferase-expressing cells were selected with 1 μg/ml puromycin.

2.2. Nanoparticle preparation and drug loading

Poly(ethylene glycol)-ε-poly(caprolactone) (PEG-PCL) block copolymer with molecular weight 5–5.5 kDa was purchased from Polymer Source (Montreal, QC, Canada). PX866 and wortmannin were purchased from LC laboratories (Woburn, MA). SN-38 was purchased from Selleckchem (Houston, TX). Acetonitrile (ACN), ethanol and water were purchased from Fisher Scientific (St. Louis, MO). PEG-PCL (100 mg, dissolved in ethanol) was mixed with drugs (10 mg, dissolved in ethanol) in a round bottom flask. The mixed solution was evaporated at reduced pressure to remove solvent and create a thin film. Polymer and drug were then reconstituted in water and sonicated for 5 min to form micelles. The micelle solution was centrifuged to remove free drug and other insoluble impurities. The supernatant containing drug-loaded nanoparticles was removed and collected by freeze-drying. The diameter and surface charge of PNPs were determined by dynamic light scattering (DLS, Zetasizer Nano ZS, Malvern, UK), and polydispersity index (PDI) of particle size was calculated by the equipped software. Alexa Fluor 546™ NHS Ester (Succinimidyl Ester) was purchased from Thermo Fisher Scientific (Waltham, MA).

2.3. HPLC PX866 quantification

Drug loading in micelles was quantified by high-performance liquid chromatography (HPLC; Agilent XDB-C18, 1 ml/min, 60:40 ACN:water with 0.1% formic acid, retention time 2.40 min). HPLC was also used to quantify PX866 in lung, liver and kidney tissue samples from mice treated with PX866-loaded micelles. Tissue samples from healthy mice were spiked with varying amounts of PX866 to create a calibration curve for drug. Drug was

extracted from spiked tissue samples by homogenizing tissues in acetonitrile for 10 min. The tissue samples were centrifuged for 20 min at 14,500 RPM to remove acetonitrile-insoluble proteins and other cell debris from solution. Wortmannin (40 μg), a structural analog of PX866, was added to each extracted sample as an internal standard. Calibration curves for PX866 extracted from tissue samples were used to quantify drug in tissue from treated mice 4 h post-treatment. PX866 in all extracted samples was quantified by HPLC using multi-step gradient (0 to 2 min, 10% ACN; 2 to 5 min increase to 40% ACN, 5 to 8 min, 40% ACN; 8 to 10 min, increase to 60% ACN; 10 to 13 min, 60% ACN; 13 to 16 min, increase to 90% ACN; 16 to 16.5 min, 90% ACN; 16.5 to 17 min, decrease to 10% ACN; 17 to 19 min, 10% ACN) to separate hydrophobic cell debris (7.2 min, 200 nm), wortmannin (10.42 min, 200 nm) and PX866 (11.29 min, 200 nm). Lung, liver and kidney tissue calibration curves had a detection limit of 10 ng/ml PX866. Drug concentrations were normalized to the mass of collected tissue and percent of initial PX866 dose.

2.4. Patient-derived xenograft (PDX) engraftment into SCID mice and lung metastasis models

Male athymic NCr nude, Swiss-Webster and BALB/C mice between 6 and 8 wks of age were purchased from Taconic (Hudson, NY). NOD-scid IL2Rgamma^{null} mice were purchased from the Jackson Laboratory (Bar Harbor, ME). Housing for these animals was maintained in a HEPA-filtrated environment within sterilized cages with 12 h light/12 h dark cycles. All animal procedures were conducted with approval of and in compliance with University of Kentucky Institutional Animal Care and Use Committee. The original patient CRC tumor (F0 generation) was divided and implanted into the flank of a NOD scid gamma mouse (The Jackson Laboratory; 005557) mouse. When the tumors grew to 1 cm^3, each tumor (F1 generation) was resected, divided into 2-mm^3 pieces and implanted into 5 mice (F2 generation).

For intravenous injection of CRC cells, athymic NCr nude or BALB/C mice were anesthetized with isoflurane (induction 4%, maintenance 2%). The viability of cells used for inoculation was > 95% as determined by Vi-CELL™ XR (Beckman Coulter). Gentle pressure was applied to the inoculation site until there was no visible sign of bleeding. Lung tissues were preserved for histological examination by fixation in 10% buffered formalin followed by paraffin embedding.

2.5. In vivo imaging

Macroscopic fluorescent imaging (Alexa Fluor 546, Ex = 535 nm, Em = 580 nm) was carried out on IVIS Spectrum station (Caliper Life Sciences; Hopkinton, MA). Composite images obtained were comprised of black and white digital photos with an overlay of images reflecting fluorescent activity. The density map, measured as photons/s/cm^2/sr (p/s/cm^2/sr), was created using the Living Image 3.1 (Caliper Life Sciences; Hopkinton, MA) software and represented as a color gradient centered at the maximal spot. GFP fluorescence imaging was performed using an LT-9500 Illumatool/TLS (Lightools Research, Encinitas, CA), equipped with an excitation source (470 nm) and filter plate (515 nm).

2.6. In vivo selection of CRC lung metastasis

Liberase DH (05401054001; Roche Applied Science) was resuspended in sterile water to 2.5 mg/ml concentration and stored in single-use 100 μl aliquots at −80 °C. Collagenase/Hyaluronidase (07912; StemCell Technologies) was aliquoted into single-use 250 μl aliquots and stored at −80 °C. Metastatic tumors were collected from mice and placed into complete cell culture media supplemented with 1× Gibco® Antibiotic-Antimycotic (15240–062; Life Technologies) for transportation. Metastatic tumor fragments were minced into 2 mm cubes using scissors and digested in 50 μg/ml Liberase DH (100 μl) and 0.5× Collagenase/Hyaluronidase (250 μl), diluted in 5 ml of McCoy5A serum free media for 4 h at 37 °C with gentle agitation by magnetic stirring bar. No undigested tissue was observed. Digested cells were washed twice with complete cell culture media and transferred into 10% FBS McCoy5A media supplemented with 1× Gibco® Antibiotic-Antimycotic and 100 μg/ml Primocin (ant-pm-1; InvivoGen). Cells harvested from these cultures were injected intravenously into another set of nude mice.

2.7. Western blot analysis and antibodies

Total protein lysates (20 μg) were resolved on a 4–12% bis-tris gel and transferred to Immobilon PVDF transfer membranes. Membranes were incubated for 40 min at room temperature in blocking solution (TRIS-buffered saline containing 5% nonfat dried milk and 0.1% Tween 20), followed by an overnight incubation in primary antibodies at 4 °C. Membranes were then washed 3 times and incubated with horseradish peroxidase–conjugated secondary antibodies for 1 h. After 3 additional washes, the immune complexes on the membranes were visualized by ECL detection. The following antibodies were purchased and utilized in our study: Cell Signaling (Danvers, MA): phospho-Akt (Ser473) (Western blot; #4058; 1:1000), total Akt (Western blot; #2920; 1:1000), PARP (Western blot; mAb #9532; 1:1000). BD (San Jose, California): phospho-Akt (Immunohistochemistry; Ser473; 1:100). Abcam (Cambridge, MA): Akt2 (Immunohistochemistry; #55391; 1:500), cyclin D1 antibody [EPR2241] (ab134175). Mouse monoclonal anti-β-actin antibody was obtained from Sigma-Aldrich (St. Louis, MO).

2.8. Immunohistochemistry

Immunohistochemistry (IHC) was performed as previously described [20]. Briefly, slides were deparaffinized in xylene, rehydrated, incubated for 15 min with fresh 0.3% hydrogen peroxide, washed with PBS, and heated to 95 °C in 10 mM citrate buffer (pH 6.0; 30 min) for Akt1 and Akt2 antibodies staining. Antigen retrieval for slides stained with pAkt (S473) antibody was performed in Tris-EDTA buffer (10 mM Tris Base, 1 mM EDTA Solution, 0.05% Tween 20, pH 9.0). Sections were blocked in serum free protein block (Dako) and treated with biotin blocking system (Dako); primary antibody was incubated for 12 h at 4 °C, washed with TBST (Tris-Buffered Saline and Tween 20) and incubated with secondary antibody (60 min; RT). pAkt (Ser473), Akt1 and Akt2 antibodies were used at a concentration of 1:100 in DAKO antibody diluent. All sections were counterstained with hematoxylin and observed by light microscopy. For negative controls, primary antibody was omitted from the above protocol. The number of positive cells was visually evaluated in each core by a pathologist (Dr. E-Y L.) and the staining intensity was classified using a

semi-quantitative seven-tier system developed by Allred et al. [21,22] The system assesses the percentage of positive cells (none = 0; < 10% = 1; 10% to 50%, =2; > 50% = 3) and intensity of staining (none = 0; weak = 1; intermediate = 2; and strong = 3).

2.9. Confocal microscopy

Tissue samples were fixed in 4% paraformaldehyde (Polysciences; 18,814) with 10% sucrose (Sigma-Aldrich; St. Louis, MO) for 12 h at 4 °C and embedded into OCT on dry ice (Tissue-Tek; Andwin Scientific, Schaumburg, IL). Frozen sections of tissues (10 μm section thickness) were dried overnight in the dark, washed in RT PBS, stained with Hoechst 33,342 (Life Technologies; H21492; 0.5 μg/ml; PBS) nuclear stain and mounted in aqueous ultramount permanent mounting medium overnight (Dako; S1964).

2.10. Statistical analysis

Paired *t*-test was used to determine differences in drug concentration between lung *versus* kidney and lung *versus* liver measured from the same mouse.

3. Results

3.1. Akt (Ser473) activation in CRC lung metastasis patient samples

To investigate the clinical significance of PI3K activation in CRC lung metastasis we analyzed patient samples for pAkt, Akt1 and Akt2 expression in lung metastases (n = 10). Samples were selected from 137 metastatic CRC cases that underwent resection at the University of Kentucky Markey Cancer Center for CRC metastases from January 1, 2003 to January 1, 2013. From this cohort, we identified 10 patients with CRC lung metastases (Fig. 1A, B). Out of 10 identified patients with CRC lung metastasis, 5 patients had surgical resection of both primary and metastatic CRC. (Supplemental Fig. 1). The number of positive cells was visually evaluated in each core by a pathologist and the staining intensity was classified using a semi-quantitative seven-tier system developed by Allred et al. [21,22]. The system assesses the percentage of positive cells (none = 0; < 10% = 1; 10% to 50%, =2; > 50% = 3) and intensity of staining (none = 0; weak = 1; intermediate = 2; and strong = 3). Our results demonstrate high pAkt (S473) and Akt2 expression (score 5–6) in all CRC lung metastasis samples (Fig. 1A, B). Normal lung cells demonstrated predominantly cellular membrane staining for pAkt, Akt1 and Akt2 protein (Supplemental Fig. 1A). Analysis of matched primary CRC tumor and metastatic lung lesions demonstrate that pAkt (S473) is overexpressed in primary CRCs and that pAkt (S473) overexpression profiles of primary CRCs are maintained in their distant metastases (Supplemental Fig. 1A, B). Therefore, targeted therapy with PI3K/Akt signaling pathway inhibitors may have a significant therapeutic potential in a large proportion of patients with CRC lung metastasis.

3.2. Lung accumulation of PNPs

All PNPs showed a sub-100 nm particle size and neutral surface charge, which are suitable for nanoparticle-mediated drug delivery to tumors. Empty micelles were 65.70 nm in average diameter (PDI = 0.18) with a neutral surface charge of −0.0213 mV. The particle size decreased slightly after drug loading while the surface charge remained neutral. Wort PNPs showed a 41.35 nm diameter (PDI = 0.35) and −0.494 mV surface charge in average.

PX866 PNPs were 41.35 nm (PDI = 0.11) and 0.00228 mV in diameter and surface charge, respectively (Supplemental Fig. 2A). TEM, DLS, *in vitro* degradation kinetics, subcytotoxic dose were described in previous publications [23,24]. PNPs showed a loading efficiency of 20% (wt/wt), and their maximum loading attained was 4% of Wort/PX866 by weight. We designed PNP with a short drug release half-life of 1.8 ± 0.4 h to deliver the therapeutic payload in a first-pass organ after intravenous (iv) injection (Supplemental Fig. 2B, C). The distribution pattern of PNPs was evaluated with macroscopic organ and confocal tissue imaging, Western blot evaluation of PI3K inhibition in organ tissues and HPLC bioanalytical measurement of PX866 accumulation in tissues. Nanoparticles were labeled with the fluorescent reagent Alexa546 and administered iv to determine nanoparticle accumulation patterns in normal organs and CRC PDX tumors. Accumulation of fluorescently-labeled PNPs was evaluated at 1 h, 4 h, 8 h, and 24 h and demonstrated rapid delivery of the nanoparticle load to lung tissue. CRC PDX tumors showed minimal accumulation of fluorescent reagent at the 24 h timepoint. (Fig. 2A, B). PNPs were loaded with pan-PI3K inhibitors and administered as a single iv dose. PI3K pathway activation was assessed in lung, liver, kidney protein extracts by Western blot analysis of pAkt (S473) expression; a decrease in pAkt (S473) expression was detected in lung tissues only (Fig. 3A, B). Confocal imaging of frozen tissue sections demonstrated strong fluorescence in lungs and an absence of significant fluorescent signal in CRC PDX tumors and kidneys. Minimal fluorescence was detected in liver tissue (Fig. 3C). HPLC analysis also confirmed that the nanoparticles accumulate mainly in the lungs (Supplemental Fig. 2C). These results demonstrate that PNPs can deliver a high dose of drugs to lung tissue and lung metastases, and to spare the kidney and liver.

3.3. Pre-clinical test of pan-PI3K PNPs

To evaluate the potential for clinical utility of PNP Wort or PX866, we studied its efficacy *in vivo* using a murine model of CRC lung metastasis. BALB/C mice were injected iv with CT26 GFP cells and treated once a day (qd) with Wort and PX866 PNP. Treatment with pan-PI3K loaded PNPs resulted in suppression of lung metastasis growth (Fig. 4A, B). A major limitation of pan-PI3K inhibitors as cancer therapeutic agents is the systemic toxicity [25]. We hypothesized that a PNP formulation of Wort would significantly reduce toxicity. Swiss-Webster mice were treated with empty PNPs or Wort PNPs every day for 7 d. Previous studies showed weight loss and growth retardation in mice that receive intraperitoneal injection or oral Wort formulation compared to their sex- or genotype-matched controls [26]. Our data showed that daily PNP Wort administration had no effect on body weight, indicating a significantly lower toxicity profile for PNP-delivered drugs (Supplemental Fig. 2D). Next, we treated Swiss-Webster mice for 7 days qd with empty PNPs, Wort PNPs and PX866 PNPs and analyzed effect of qd treatment on normal tissue (Supplemental Fig. 2E; Supplemental Table 1). Treatment with empty PNPs had no deleterious effect on lung, liver, kidney or spleen. Wort and PX866 PNPs had minor reversible effect on normal liver tissue and no effect on normal lung, kidney or spleen. Western blot analysis of lung tissues samples demonstrated that Akt (Ser473) restores to original level 24 h after last treatment with Wort and PX866 PNPs, and no PARP activation was observed in empty PNP treatment group.

The greatest therapeutic potential of PI3K pathway inhibition lies in its ability to potentiate the effects of chemotherapy [27,28]. Our results show that pan-PI3K PNPs efficiently suppress CRC lung metastasis proliferation and growth (Fig. 4A, B). To evaluate pan-PI3K inhibitors in a human pre-clinical model of CRC lung metastasis, we performed an *in vivo* selection procedure to establish a CRC cell line that is highly metastatic to the lung; GFP imaging of mice injected with HT-29 LuM2 demonstrated a 100% metastatic penetrance at 4 wks compared to injection of the parental cell line at 14 wks (Fig. 5A). We hypothesized that high dose of PX866 in target tissues or addition of chemotherapeutic agents, in combination with PX866, would have the potential to clear CRC metastatic lesions. Comparison of PI3K inhibition in HT-29 LungM3 cells *in vitro* by PX866 dissolved in DMSO or PX866 PNPs showed longer duration of PI3K inhibition and induction of apoptosis after PX866 PNPs treatment (Supplemental Fig. 3A, B). High dose of PX866 PNPs treatment caused rapid induction of apoptosis (Supplemental Fig. 3C). SN-38, the active metabolite of irinotecan, is a poorly water soluble, very potent chemotherapeutic agent for a variety of human cancers [29,30]. SN-38 has not yet been used in a clinical setting to treat human cancer patients due to the inability to administer sufficient quantities in a pharmaceutical formulation [31]. We compared the effect of SN-38 treatment *in vitro* on HCT116 and HT-29 LungM3 cell lines and show that HT-29 LungM3 cell line was relatively resistant to SN-38 treatment (Supplemental Fig. 4A). A PNP formulation of SN-38 was prepared and tested *in vitro* in combination with PX866 PNPs treatment of HT-29 LungM3 cells. Western blot analysis demonstrated that SN-38 and PX866 combination induced apoptosis in HT-29 LungM3 at low doses and identified a successful combination strategy. Induction of apoptosis *in vitro* was observed after simultaneous inhibition of PI3K and SN-38 treatment or after initial SN-38 treatment followed by PI3K inhibition (Supplemental Fig. 4B). Next, CRC lung metastasis was established after iv injection of HT-29 LuM3 cells. The PNPs loaded with PX866 and SN-38 were administered iv 72 h after HT-29 LuM3 cells injection every day for 4 d and continued every 3 d for 26 d. PX866 + SN−38 combination treatment was administered iv 72 h after HT-29 LuM3 cells injection every day for 4 days. Treatment with PX866 PNPs suppressed CRC lung metastasis growth; treatment with SN-38 PNPs cleared CRC lung metastasis. (Fig. 5B). Combination treatment every day for 4 d was also highly efficient in clearing CRC lung metastasis, but had a profound deleterious effect on normal lung tissue (Supplemental Fig. 4C). These results demonstrate that PI3K inhibition efficiently suppresses proliferation of CRC lung metastasis and SN-38 nanoparticle drug delivery completely eliminates CRC lung metastasis.

4. Discussion

Metastatic malignant neoplasms are the most common form of secondary lung tumors. Secondary lung tumors are neoplasms that can arise within the lung or outside the lung, with the metastases traveling through the bloodstream or lymphatic system or by direct extension to reach their destination. Lung metastases are identified in 30–55% of all cancer patients, though their prevalence varies according to the type of primary cancer [32,33]. In these circumstances, removing the visible tumors by surgery is usually insufficient and chemotherapy is the only treatment of choice. A five-year progression-free survival for patients with metastatic cancer to the lungs is uncommon. Secondary lung metastasis is one

of the most significant problems in the field of oncology and there is a need for an effective and reliable solution to translate highly promising *in vitro* therapeutics into clinical practice. Here, we used CRC lung metastasis as a model disease to evaluate novel nanocarrier and demonstrate that lung drug delivery is a viable treatment strategy for secondary lung metastasis.

Aberrant PI3K pathway activation is one of the most frequent occurrences in human cancer and is critical for tumor progression [14]. The PI3K signaling pathway has attracted a great deal of interest due to its involvement in a large proportion of human tumors; however, preclinical studies and clinical trials with other kinase-based therapies suggest that partial inhibition of the signal due to limitations in the dosing could account for the limited clinical responses. For example, preclinical studies of the pan-Class I PI3K inhibitor pictilisib demonstrated that quick PI3K inhibition resulted in growth arrest in tumor xenografts, but had limited antitumor activity as a single agent [34]. In another clinical trial, PI3K inhibitors were only able to induce modest target inhibition with daily administration of the maximum tolerated dose [35]. Our results also showed that the anticancer effect of PI3K inhibition is dose dependent and required a higher dose to induce apoptosis in cancer cells. The inability to achieve tolerated therapeutic dosages to target tumor cells and the severe side effects on liver, kidney and gastrointestinal tract are major factors limiting the success of previous cancer metastasis treatment with PI3K/Akt inhibitors [36]. PNPs offer a solution to allow for high-dose delivery of pharmaceuticals to target lung metastasis [37,38]. We engineered PNPs encapsulating hydrophobic PI3K inhibitors and demonstrated remarkable improvement in drug cytotoxicity, solubility, and the duration of PI3K inhibition *in vitro* and *in vivo* compared to free PI3K inhibitors. As a proof of principle, we evaluated the clinical potential of compounds that had previously failed clinical development due to pharmacologic challenges. We were able to successfully deliver a high dose of PI3K/Akt inhibitors using PNPs and to limit systemic toxicity with a resultant high drug concentration in lung tissue with relative sparing of the GI tract, kidneys, and liver.

Targeting nanoparticles to cancer cells for improved therapy is a popular concept. However, a recent review of the literature from the past decade showed that only 0.7% of the administered nanoparticle dose is actually delivered into a tumor [9]. A reimagining of conventional nanoparticles is needed to determine successful drug delivery into metastatic tumors. One of the most challenging problems in the targeted delivery of nanoparticles is to develop high-quality targeting ligands that can give rise to more specific accumulation of nanoparticles in tumors than in other tissues. Here, we used polymeric nanoparticles to achieve high drug concentration in lung tissue affected by metastatic disease. Lung drug delivery was confirmed multiple times in different timepoint, strains of mice (athymic nude, SCID, Balb/C, C57BL/6 J) and by various methods (Western blot analysis of organs protein tissue extracts, macroscopic IVIS imaging, microscopic confocal imaging and HPLC). Currently, we cannot explain drug delivery to lung tissue and plan to introduce modifications to nanoparticles used in the study to identify properties of the nanoparticles play role in drug delivery to lung tissue. Using a highly-reproducible and effective CRC lung metastasis model developed in our laboratory, we show that nanocarrier drug delivery to lung tissue was sufficient for the inhibition of CRC metastasis growth or complete elimination of CRC lung metastases without deleterious effects on normal lung, liver or kidney tissues.

Therefore, it is possible to use commercially available PEG-PCL polymer to design tunable biomaterials and achieve PNP accumulation in parenchymal organs commonly affected by metastatic disease.

In conclusion, we report the development of a PNP formulation of pan-PI3K inhibitors, wortmannin and PX866, and also demonstrate the potential of SN-38 against CRC lung metastases. PNPs were found to be soluble and stable and to accumulate in lung tissue. Our work also addresses, at least in part, some of the major barriers to translating otherwise promising small molecules from the laboratory to the clinic. Most importantly, this strategy can be applied to treat lung metastases that originate from various cancers. Moreover, this strategy offers the possibility of delivering effective therapies to the lung without toxicity that is associated with systemic delivery.

Supplementary Material

Refer to Web version on PubMed Central for supplementary material.

Acknowledgments

The authors thank the Markey Cancer Center's Research Communications Office for help with manuscript preparation. We also thank the Biostatistics and Bioinformatics and the Biospecimen Procurement and Translational Pathology Shared Resource Facilities of the Markey Cancer Center for statistical analysis and histologic assessment, respectively. The contents of this manuscript are solely the responsibility of the authors and do not necessarily represent the official views of the grant funding agencies. This study was supported by grants P30 CA177558, R01 CA195573, and R01 DK048498 from the National Institutes of Health (NIH).

References

1. Siegel RL, Miller KD, Jemal A. Cancer statistics, 2017. CA Cancer J Clin. 67 (1) 2017; :7–30. [PubMed: 28055103]
2. Rusch VW. Pulmonary metastasectomy. Current indications. Chest. 107 (Suppl 6) 1995; :322s–331s. [PubMed: 7781414]
3. Villeneuve PJ, Sundaresan RS. Surgical management of colorectal lung metastasis. Clin Colon Rec Surg. 22 (4) 2009; :233–241.
4. Mitry E, et al. Epidemiology, management and prognosis of colorectal cancer with lung metastases: a 30-year population-based study. Gut. 59 (10) 2010; :1383–1388. [PubMed: 20732912]
5. Pihl E, Hughes ES, McDermott FT, Johnson WR, Katrivessis H. Lung recurrence after curative surgery for colorectal cancer. Dis Colon Rectum. 30 (6) 1987; :417–419. [PubMed: 3595358]
6. Mohammed TL, et al. ACR Appropriateness Criteria(R) screening for pulmonary metastases. J Thorac Imaging. 26 (1) 2011; :W1–3. [PubMed: 21258219]
7. Duggan ST, Keating GM. Pegylated liposomal doxorubicin: a review of its use in metastatic breast cancer, ovarian cancer, multiple myeloma and AIDS-related Kaposi's sarcoma. Drugs. 71 (18) 2011; :2531–2558. [PubMed: 22141391]
8. Barenholz Y. Doxil(R)—the first FDA-approved nano-drug: lessons learned. J Control Release. 160 (2) 2012; :117–134. [PubMed: 22484195]
9. Wilhelm S, et al. Analysis of nanoparticle delivery to tumours. Nat Rev Mater. 1 2016; :16014.
10. Venditto VJ, Szoka FC. Cancer Nanomedicines: so many papers and so few drugs! Adv Drug Deliv Rev. 65 (1) 2013; :80–88. [PubMed: 23036224]
11. Park K. Facing the truth about nanotechnology in drug delivery. ACS Nano. 7 (9) 2013; :7442–7447. [PubMed: 24490875]
12. Johnson SM, et al. Novel expression patterns of PI3K/AKT/mTOR signaling pathway components in colorectal cancer. J Am Coll Surg. 210 (5) 2010; :767–778. [PubMed: 20421047]

13. Vanhaesebroeck B, Stephens L, Hawkins P. PI3K signalling: the path to discovery and understanding. Nat Rev Mol Cell Biol. 13 (3) 2012; :195–203. [PubMed: 22358332]
14. Thorpe LM, Yuzugullu H, Zhao JJ. PI3K in cancer: divergent roles of isoforms, modes of activation and therapeutic targeting. Nat Rev Cancer. 15 (1) 2015; :7–24. [PubMed: 25533673]
15. Dibble CC, Cantley LC. Regulation of mTORC1 by PI3K signaling. Trends Cell Biol. 25 (9) 2015; :545–555. [PubMed: 26159692]
16. Hu Y, et al. Effects of PI3K inhibitor NVP-BKM120 on overcoming drug resistance and eliminating cancer stem cells in human breast cancer cells. Cell Death Dis. 6 2015; :e2020. [PubMed: 26673665]
17. Isoyama S, et al. Establishment of phosphatidylinositol 3-kinase inhibitor-resistant cancer cell lines and therapeutic strategies for overcoming the resistance. Cancer Sci. 103 (11) 2012; :1955–1960. [PubMed: 22925034]
18. Ulery BD, Nair LS, Laurencin CT. Biomedical applications of biodegradable polymers. J Polym Sci B Polym Phys. 49 (12) 2011; :832–864. [PubMed: 21769165]
19. Lupi M, et al. A biodistribution study of PEGylated PCL-based nanoparticles in C57BL/6 mice bearing B16/F10 melanoma. Nanotechnology. 25 (33) 2014; :335706. [PubMed: 25074670]
20. Rychahou PG, Jackson LN, Silva SR, Rajaraman S, Evers BM. Targeted molecular therapy of the PI3K pathway: therapeutic significance of PI3K subunit targeting in colorectal carcinoma. Ann Surg. 243 (6) 2006; :833–842. [PubMed: 16772787]
21. Allred DC, et al. Association of p53 protein expression with tumor cell proliferation rate and clinical outcome in node-negative breast cancer. J Natl Cancer Inst. 85 (3) 1993; :200–206. [PubMed: 8423624]
22. Allred DC, Harvey JM, Berardo M, Clark GM. Prognostic and predictive factors in breast cancer by immunohistochemical analysis. Mod Pathol. 11 (2) 1998; :155–168. [PubMed: 9504686]
23. Huang MH, et al. Degradation and cell culture studies on block copolymers prepared by ring opening polymerization of epsilon-caprolactone in the presence of poly(ethylene glycol). J Biomed Mater Res A. 69 (3) 2004; :417–427. [PubMed: 15127388]
24. Grossen P, Witzigmann D, Sieber S, Huwyler J. PEG-PCL-based nanomedicines: a biodegradable drug delivery system and its application. J Control Release. 260 (Suppl C) 2017; :46–60. [PubMed: 28536049]
25. Ihle NT, et al. Molecular pharmacology and antitumor activity of PX-866, a novel inhibitor of phosphoinositide-3-kinase signaling. Mol Cancer Ther. 3 (7) 2004; :763–772. [PubMed: 15252137]
26. MacKay KB, Lowenson JD, Clarke SG. Wortmannin reduces insulin signaling and death in seizure-prone Pcmt1−/− mice. PLoS One. 7 (10) 2012; :e46719. [PubMed: 23071621]
27. Moon DG, et al. NVP-BEZ235, a dual PI3K/mTOR inhibitor synergistically potentiates the antitumor effects of cisplatin in bladder cancer cells. Int J Oncol. 45 (3) 2014; :1027–1035. [PubMed: 24969552]
28. Clark AS, West K, Streicher S, Dennis PA. Constitutive and inducible Akt activity promotes resistance to chemotherapy, Trastuzumab, or Tamoxifen in breast cancer cells. Mol Cancer Ther. 1 (9) 2002; :707. [PubMed: 12479367]
29. van Ark-Otte J, et al. Determinants of CPT-11 and SN-38 activities in human lung cancer cells. Br J Cancer. 77 (12) 1998; :2171–2176. [PubMed: 9649129]
30. Jansen WJ, et al. CPT-11 in human colon-cancer cell lines and xenografts: characterization of cellular sensitivity determinants. Int J Cancer. 70 (3) 1997; :335–340. [PubMed: 9033637]
31. Ugwu S, et al. Preparation, characterization, and stability of liposome-based formulations of mitoxantrone. Drug Dev Ind Pharm. 31 (2) 2005; :223–229. [PubMed: 15773289]
32. Crow J, Slavin G, Kreel L. Pulmonary metastasis: a pathologic and radiologic study. Cancer. 47 (11) 1981; :2595–2602. [PubMed: 7260854]
33. Seo JB, Im J-G, Goo JM, Chung MJ, Kim M-Y. Atypical pulmonary metastases: Spectrum of radiologic findings. Radiographics. 21 (2) 2001; :403–417. [PubMed: 11259704]
34. Sarker D, et al. First-in-human phase I study of Pictilisib (GDC-0941), a potent pan-class I phosphatidylinositol-3-kinase (PI3K) inhibitor, in patients with advanced solid tumors. Clin Cancer Res. 21 (1) 2015; :77–86. [PubMed: 25370471]

35. Bendell JC, et al. Phase I, dose-escalation study of BKM120, an oral pan-class I PI3K inhibitor, in patients with advanced solid tumors. J Clin Oncol. 30 (3) 2012; :282–290. [PubMed: 22162589]

36. Hammadi SA, Almarzooqi S, Abdul-Kader HM, Saraswathiamma D, Souid A-K. The PI3Kδ inhibitor idelalisib suppresses liver and lung cellular respiration. Int J Physiol Pathophysiol Pharmacol. 7 (3) 2015; :115–125. [PubMed: 26823960]

37. Raynaud FI, et al. Biological properties of potent inhibitors of class I phosphatidylinositide 3-kinases: from PI-103 through PI-540, PI-620 to the oral agent GDC-0941. Mol Cancer Ther. 8 (7) 2009; :1725. [PubMed: 19584227]

38. Guillard S, et al. Molecular pharmacology of phosphatidylinositol 3-kinase inhibition in human glioma. Cell Cycle. 8 (3) 2009; :443–453. [PubMed: 19177002]

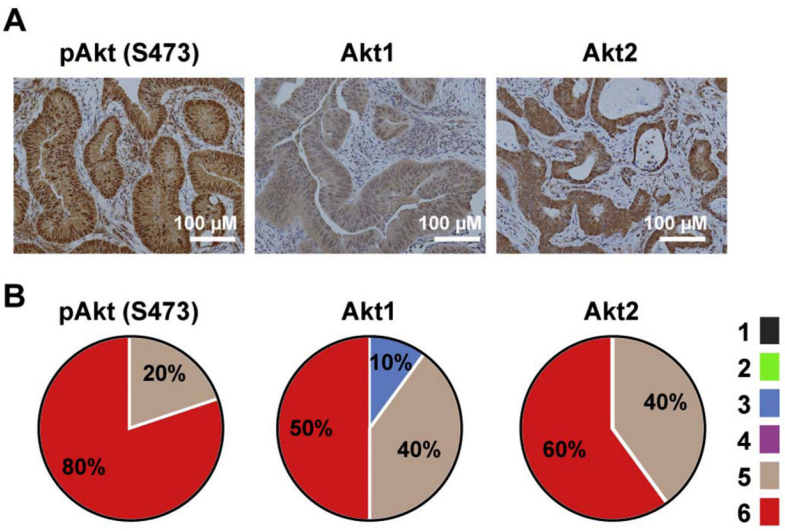

Fig. 1. Analysis of PI3K/Akt expression in CRC lung metastasis

A. Examples of immunohistochemical staining for Akt1, Akt2 and pAkt (S473) in CRC lung metastases (n = 10; magnification 20×). **B.** Positive pAkt (S473) staining of CRC was cytoplasmic or membranous or both; most positive cases showed both patterns. Differences in proportion of positive cells and intensity of staining were noted in positively stained cases and formed the basis of our grading system. Comprehensive total score that weighs both factors was calculated by summation of proportion and intensity values. High pAkt (S473) expression (score 6) was detected in 80% of CRC lung metastases.

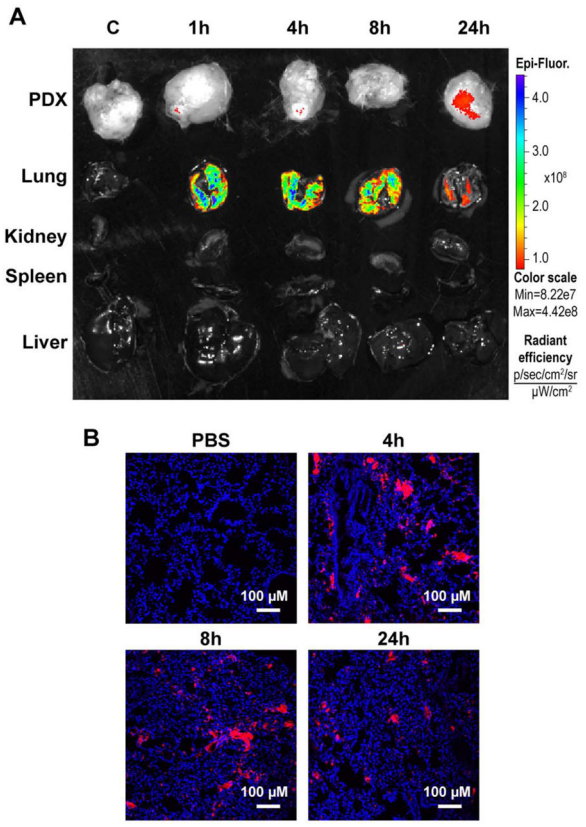

Fig. 2. Selective accumulation of polymeric nanoparticles in tissues

A. The polymeric nanoparticles loaded with Alexa546 (single 50 µg/g dose in 300 µl of PBS) were injected iv into SCID mice with CRC PDX tumors. Accumulation of fluorescently labeled pRNA nanoparticles was evaluated at 1h, 4h, 8h, and 24 h. Scale bar: fluorescent intensity. **B.** Confocal imaging of fixed frozen lung tissue sections. Control: Empty PNP. blue: DAPI; magenta: Alexa546, magnification 20×.

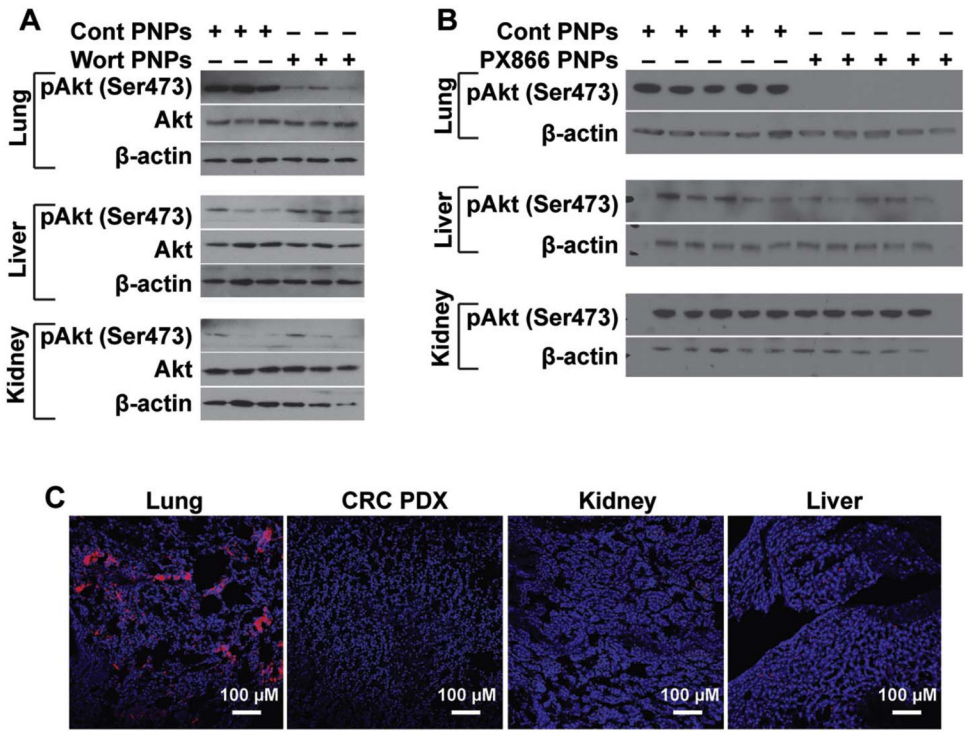

Fig. 3. Lung selective drug payload delivery

A. B. The polymeric nanoparticles loaded with pan-PI3K inhibitors (wortmannin and PX866) were administered iv (single 10 μg/g dose in 300 μl of PBS; 4h). PI3K pathway activation was analyzed in protein extracted from lung, liver, kidney tissues for pAkt (S473) expression by Western blot. C. Confocal imaging of fixed frozen tumor xenograft sections 1h after fluorescent nanoparticle iv administration (single 50 μg/g dose in 300 μl of PBS). Control: Empty PNP. blue: DAPI; magenta: Alexa546, magnification 20×.

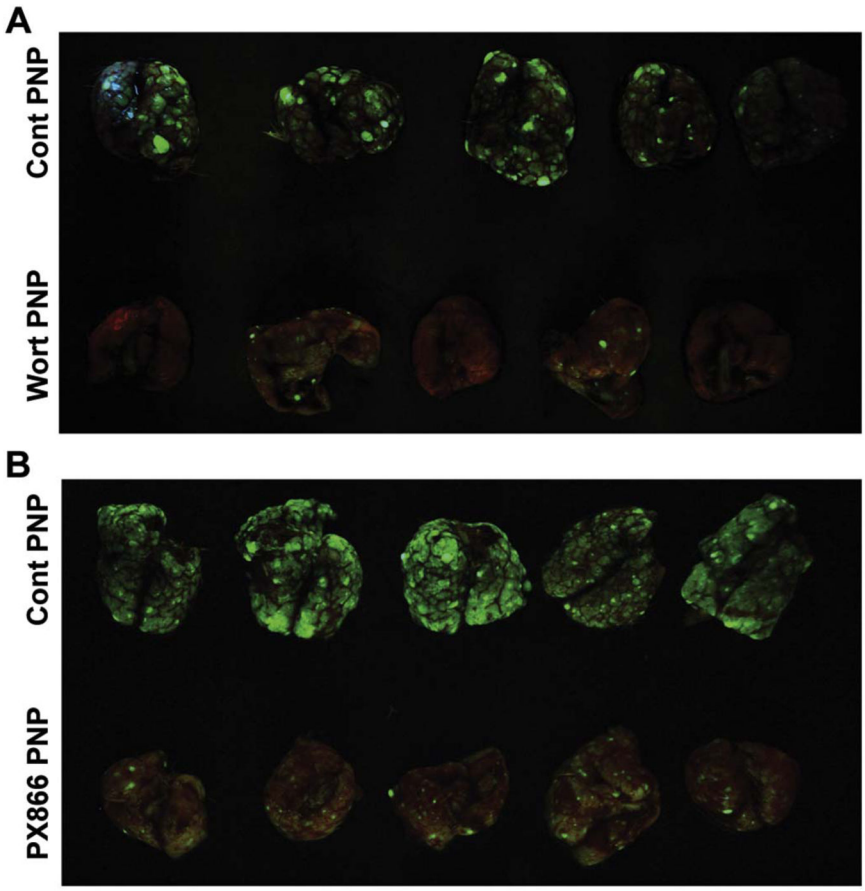

Fig. 4. CRC lung metastasis treatment with pan-PI3K loaded nanoparticles

A. B. CRC lung metastases were established after iv injection of CT26 cells (1×106 cells in 100 μl of PBS). The polymeric nanoparticles loaded with pan-PI3K inhibitors (wortmannin and PX866) were administered iv 48h after CT26 cells injection (10 μg/g dose in 300 μl of PBS, qd) 10 days. Control: Empty PNPs. Green: GFP expressing CT26 cells.

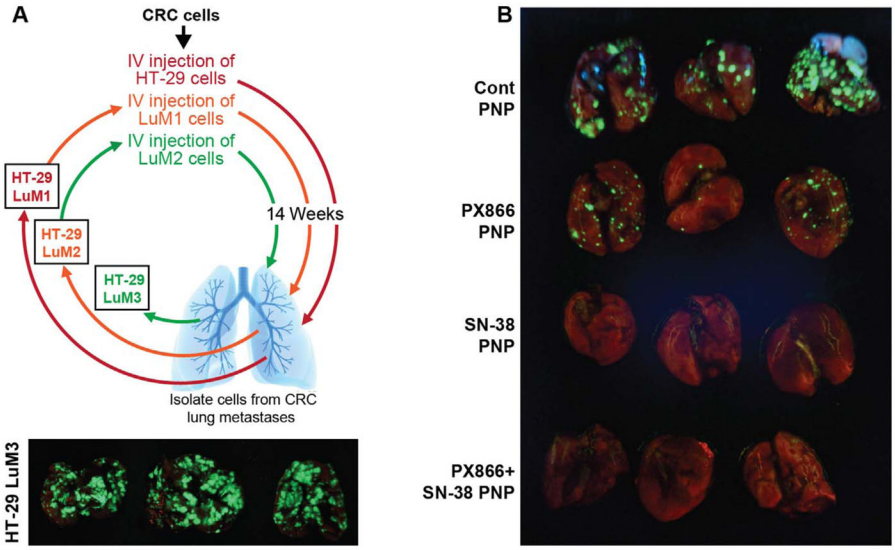

Fig. 5. CRC lung metastasis treatment with PX866 and SN-38 loaded nanoparticles

A. Illustration of metastatic CRC *in vivo* selection process. Experimental lung metastases were harvested, established in culture and designated HT-29 LuM1, LuM2 and LuM3 cell lines. **B.** CRC lung metastasis was established after iv injection of HT-29 LuM3 cells (1.5×106 cells in 100 μl of PBS). The polymeric nanoparticles loaded with PX866 and SN-38 were administered iv 72h after HT-29 LuM3 cells injection every q24h for 4 days and continued every q72h for 26 days (10 μg/g dose in 300 μl of PBS). PX866+SN−38 combination treatment was administered iv 72h after HT-29 LuM3 cells injection every q24h for 4 days (10 μg/g PX866 + 10 μg/g SN-38 mixed in 300 μl of PBS). Control: Empty PNP. Green: GFP expressing HT-29 LuM3 cells.